

**Repository of the Max Delbrück Center for Molecular Medicine (MDC)
in the Helmholtz Association**

<http://edoc.mdc-berlin.de/15654>

**Satellite microglia display spontaneous electrical activity uncorrelated
with activity of the attached neuron**

Wogram, E. and Wendt, S. and Matyash, M. and Pivneva, T. and Draguhn, A. and Kettenmann, H.

This is the final version of the manuscript. It is the peer reviewed version of the following article:

Wogram, E., Wendt, S., Matyash, M., Pivneva, T., Draguhn, A. and Kettenmann, H. (2016),
Satellite microglia show spontaneous electrical activity that is uncorrelated with activity of the
attached neuron. *Eur J Neurosci*, 43: 1523–1534. doi:10.1111/ejn.13256

which has been published in final form in:

European Journal of Neuroscience
2016 JUN ; 43(11): 1523-1534
2016 MAY 21 (first published online)
doi: [10.1111/ejn.13256](https://doi.org/10.1111/ejn.13256)

Publisher: [Wiley-Blackwell](http://www.wiley-blackwell.com)

Section: Molecular & Synaptic Mechanisms**Satellite microglia display spontaneous electrical activity uncorrelated with activity of the attached neuron**

Emile Wogram^{1,3,4}, Stefan Wendt^{1,4}, Marina Matyash¹, Tatyana Pivneva²,
Andreas Draguhn³ and Helmut Kettenmann¹

¹ Cellular Neurosciences, Max-Delbrück Center for Molecular Medicine, 13092
Berlin, Germany

² Bogomoletz Institute of Physiology, General Physiology of Nervous System
Department, 01024 Kiev, Ukraine

³ Institute of Physiology and Pathophysiology, University of Heidelberg, 69120
Heidelberg, Germany

⁴ Co-first Authors

For correspondence:

Prof. Dr. Helmut Kettenmann

Cellular Neurosciences

Max Delbrueck Center for Molecular Medicine in the Helmholtz Society

Robert-Roessle-Strasse 10

13125 Berlin

Germany

kettenmann@mdc-berlin.de

- 33 pages, 7 figures, 2 supplementary figures, 1 table
- 7621 words are in the whole manuscript; 203 in the Abstract; 489 in the Introduction.

Running Title: Spontaneous electrical activity in microglia

Key words: satellite microglia, identified neurons, electrical activity, membrane potential

Abstract

Microglia are innate immune cells of the brain. We have studied a subpopulation of microglia, called satellite microglia. This cell type is defined by a close morphological soma-to-soma association with a neuron, indicative of a direct functional interaction. Indeed, ultrastructural analysis revealed closely attached plasma membranes of satellite microglia and neurons. However, we found no apparent morphological specializations of the contact and biocytin injection into satellite microglia showed no dye-coupling with the apposed neuron or any other cell. Likewise, evoked local field potentials or action potentials and postsynaptic potentials of the associated neuron did not lead to any transmembrane currents or non-capacitive changes in the membrane potential of the satellite microglia in the cortex and hippocampus. Both satellite and non-satellite microglia, however, showed spontaneous transient membrane depolarizations which were not correlated with neuronal activity. These events could be divided into fast and slow rising depolarisations, which exhibited different characteristics in satellite and non-satellite microglia. Fast and slow rising potentials differed with regard to voltage dependence. The frequency of these events was not affected by application of TTX, but fast rising event frequency decreased after application of GABA. We conclude that microglial cells show spontaneous electrical activity uncorrelated with the activity of adjacent neurons.

Introduction

Microglia are innate immunocompetent cells of the central nervous system. Recent evidence indicates that they also play important roles in the developing and adult brain (for review see Kettenmann *et al.*, 2013). Microglial cells are more or less equally distributed, and each cell occupies a defined volume of brain parenchyma (Lawson *et al.*, 1990). In the normal brain they are characterized by a distinct ramified morphology with small cell bodies and branched processes which constantly scan their environment (Nimmerjahn *et al.*, 2005; Kettenmann *et al.*, 2011). They appear to play a role for synaptic function in the adult brain where microglial processes regularly attach to synapses and rest for about 5 minutes before continuing their constant screening process (Wake *et al.*, 2009). It has been suggested that microglia sense synaptic activity since they express a plethora of neurotransmitter and neuromodulator receptors in culture and in acute brain slices (Kettenmann *et al.*, 2011; Pannell *et al.*, 2014). Small transmembrane currents triggered by activation of receptors can induce significant changes in membrane potential, due to the high input resistance of microglial cells (Boucsein *et al.*, 2000; Newell & Schlichter, 2005).

Nearly a century ago Pío del Río Hortega described a subpopulation of microglial cells in the rabbit brain. Cell body and processes of these cells are in close contact with a neuronal cell body, and he termed these cells satellite microglia (Del Río Hortega, 1919). In the present study we recorded membrane currents and potentials from satellite microglial cells and from their attached neuron to directly test for potential interactions. While we did not find correlated neuronal and microglial activity, we identified a novel form of intrinsic, spontaneous microglial electrical activity.

Methods

Animals

All mice used in this study were on C57BL/6 genetic background. If not stated otherwise MacGreen mice (Charles River, Germany) expressing EGFP (enhanced green fluorescent protein) under colony stimulating factor 1 receptor promoter (Sasmono *et al.*, 2003) were used to detect microglia in acute isolated brain slices. Mice were kept under a 12-hour/12-hour dark-light cycle with food and water supply ad libitum. All experiments were performed according to the guidelines of the German law for animal protection. The animal experiments and care protocols were approved by the Landesamt für Gesundheit und Soziales, Berlin (X9023/12).

Slice preparation

Acute brain slices were prepared from 6-12 weeks old or 2-3 weeks old (for dual patch-clamp recordings) male and female MacGreen mice. The animals were sacrificed by dislocation of the vertebra and the brain was immediately removed and transferred into ice cold artificial cerebrospinal fluid (ACSF) gassed with 95 % O₂ / 5 % CO₂. The ACSF contained (mM): NaCl, 134; KCl, 2.5; MgCl₂, 1.3; CaCl₂, 2; K₂HPO₄, 1.25; NaHCO₃, 26; D-glucose, 10; pH 7.4; with measured osmolarity of 310-320 mOsm/L. The brain was then fixed on the stage of a vibratome (Leica SM2000R or Leica VT1200S, Nussloch, Germany), and 250-350 µm thick slices were cut. Isolated slices were kept for experiments at room temperature (RT) in gassed ACSF for a maximum of 5 hours.

Electrophysiological recordings

Slices were transferred into the submerged patch-clamp chamber which was perfused with gassed ACSF at room temperature with a velocity of 3-6 mL/min. Microglial cells were identified by their expression of EGFP whereas neurons were identified by their optical appearance in bright field microscopy and by their ability to generate action potentials. Micropipettes were pulled from borosilicate glass capillaries with 4-8 M Ω resistances for whole-cell patch-clamp recordings of microglial cells and with 2-3 M Ω for neurons. The standard intracellular solution contained (mM): KCl, 130; MgCl₂, 2; CaCl₂, 0.5; Na-ATP, 2; EGTA, 5; HEPES, 10; pH 7.4; with measured osmolarity of 280-290 mOsm/L and sulforhodamine 101, 0.01 (SR101) (Sigma Aldrich, St. Louis, USA). A second intracellular solution with low chloride concentration was used containing (mM): KCl, 6; Potassium gluconate 126; MgCl₂, 2; CaCl₂, 0.5; Na-ATP, 2; EGTA, 5; HEPES, 10, SR 101, 0.01; pH 7.4; with measured osmolarity of 270 mOsm/L. All recordings were done with conventional patch-clamp amplifiers (EPC9/10 (HEKA Elektronik, Lambrecht, Germany) and ELC-03XS (npi, Tamm, Germany)). Whole-cell recordings with a series resistance above 65 M Ω or with unstable recording conditions were discarded. To determine the pattern of membrane currents in voltage clamp mode, a series of de- and hyperpolarising voltage pulses were applied ranging from -160 mV to 50 mV with 10 mV increment (pulse duration 50 ms). Holding potential was -70 mV for neurons and -20 mV or -70 mV for microglia (see Results). To record spontaneous depolarizing events, microglial cells were hyperpolarized to about -70 mV by constant current injection in current clamp mode and spontaneous activity was recorded for at least 5 min after a stable baseline was assured. Dual patch-clamp experiments of a neuron and its satellite microglial cell were

performed in current clamp mode or in voltage clamp mode. We first approached the neuron and established a stable patch-clamp recording.

Subsequently the apposed microglia was approached and currents were recorded. To trigger action potentials the neuron was depolarized slightly above the threshold to elicit action potentials for 800 ms.

For unipolar electrical stimulation borosilicate glass microelectrodes with $<1\text{ M}\Omega$ resistance were placed in the stratum radiatum in the CA1 region using a ISO-STIM 01D (npi electronic, Tamm, Germany) for stimulation protocols. To record extracellular field potentials, electrodes were pulled from borosilicate glass capillaries with 1-2 $\text{M}\Omega$ resistance, filled with ACSF and placed in the stratum radiatum in the CA1 region, close to stratum pyramidale. Evoked population spikes were recorded that had a half-width of less than 3 ms and a minimal amplitude of 0.5 mV. All field potential recordings were amplified 100x with the DAM 80 (World Precision Instruments, Sarasota, USA) and low-pass filtered at 10 kHz, high-pass filtered at 0.1 Hz, and digitized at 50 kHz for off-line analysis with TIDA.

The following substances were dissolved in distilled water and bath-applied for pharmacological tests (μM): CNQX, 20 (Tocris); D-AP5, 50 (Tocris); GABA, 1000 (Tocris); PPADS, 100 (Sigma Aldrich); Reactive Blue 2, 100 (Tocris); TNP-ATP, 2 (Tocris); TTX, 1-2 (Tocris).

Biocytin labelling and immunohistochemistry

Immunohistochemistry was performed on acute brain slices. Microglial cells were dialyzed via a patch electrode with a solution containing biocytin (0.5 % w/v) and SR101 (0.01 mM). Biocytin filling was assumed to be complete when

the SR101 fluorescence was visible in fine distal processes. Usually, the cells were completely stained after 15 min and the electrode was pulled off after the seal was damaged by a large hyperpolarizing current injection. Subsequently, the slices were fixed in 4 % paraformaldehyde solution in 0.1 MPB (pH 7.4) for 1 h at RT, then washed with TBS (50 mM Tris, 146 mM NaCl, pH 7.4) and submitted for combined biocytin detection using Streptavidin-Cy3 and immunolabeling. Primary anti-Iba1 (Wako, Neuss, Germany) and anti-NeuN (EMD Milipore, Darmstadt, Germany) were used to label microglia and neurons, respectively, secondary antibodies were either Alexa fluor-488 or Alexa Fluor-647 labelled (Life Technologies, Darmstadt, Germany). Immunohistochemistry was performed on free-floating brain slices. First, slices were rinsed with TBS (50 mM Tris, 146 mM NaCl, pH 7.4) under gentle agitation, then they were incubated in a detergent-containing solution (1 % Triton X-100 in TBS) followed by incubation in blocking solution (5 % BSA, 5 % donkey serum in TBS) for 1 hour at RT. Finally slices were labelled with antibodies according to a standard procedure. In brief, Streptavidin/Cy3 was diluted 1 to 200; primary NeuN antibody was diluted 1 to 400; primary Iba1 antibody was diluted 1 to 600 and all secondary antibodies were diluted 1 to 200.

Nuclei were labelled with DAPI (200 nM, in TBS). Immunolabelled slices were mounted onto glass microscope slides (Superfrost®Plus, Menzel-Glaser, Braunschweig, Germany), embedded in Vectashield mounting media (Vector Laboratories, Eching, Germany) and kept at 4 °C until image acquisition.

Confocal microscopy and 3D morphological analysis

High-resolution 3-dimensional (3D) images of cortex and hippocampus were obtained using LSM710 confocal microscope (Zeiss, Oberkochen, Germany),

equipped with a motorized table and controlled by Zen 2010 software. Z-stacks with 1 μm steps were acquired using 40 X oil immersion objective (Plan-Apochromat) with numeric aperture 1.3 and working distance 0.19 mm, pinhole size set to 1 Airy unit; 9.6 pixels per 1 μm . Rendered 3D images of microglia and neurons were obtained using Surfaces and Filament tools of Imaris 7.6.4 software (Bitplane, Zurich, Switzerland).

To visualize the contact area between a neuron and its satellite microglia, cells were labelled with Alexa Fluor-488 and biocytin/Streptavidin-Cy3, respectively; fluorescence colocalization was detected in the places of tight contacts between microglia and neuron, subsequently fluorescence co-localization analysis was performed using Imaris 7.6.4 software. In brief, with the help of ImarisColoc colocalized green (neurons) and red (microglia) pixels were segregated into a new digital fluo488/Cy3 fluorescence colocalization channel (yellow), which is displayed on volume rendered 3-dimentional fluorescence images along with original (green and red) fluorescence channels. Subsequently, on volume rendered 3-dimentional fluorescence images green and red fluorescence pixels that were located on different Z-planes are displayed in green and red, respectively, but displayed in yellow when they were located on one Z-plane.

This approach enabled us to label close contact areas between microglial and neuronal somata.

Electron microscopy of biocytin-filled microglial cells

Acute brain slices with microglia filled with biocytin via the patch pipette were fixed with 4 % paraformaldehyde and 1 % glutaraldehyde for 3 h and rinsed with PBS for 30 min. Slices were incubated overnight with ABC-Elite kit to label the biocytin-filled cells (Vector Laboratories, Inc. USA), washed with PBS and then

incubated in 1.5 mg 3,3' diaminobenzidine tetrahydrochloride (DAB) (Sigma-Aldrich) and 1 mg NiCl_2 per 1 ml PBS. The DAB reaction was stopped as soon as a dark brown reaction became visible. The slices were then washed several times and postfixed in buffered 1 % osmium tetroxide solution. They were dehydrated through graded concentrations of ethanol, pre-embedded with propylene oxide, and flat-embedded in EPON resins. Ultrathin sections were counterstained with uranyl acetate and lead citrate and examined in an electron microscope (EM910; Carl Zeiss, Oberkochen, Germany).

Statistics

Data are presented as mean \pm standard error of the mean (if normally distributed) or median \pm standard error of the median (if not normally distributed). Curve fittings with lognormal and Gaussian distributions were performed with the Multipeak Fitting Tool of Igor Pro 6.36. Statistical testing was performed with Microsoft EXCEL 2013 or R (3.2.2.). We used the Mann-Whitney U test to compare event rising and decay velocities and amplitudes and to test for significance. Kolmogorov-Smirnov test was used to compare distributions. Differences between mean event frequencies were tested for significance using paired Student's t-test. "n.s." means "not significant", * $P < 0.05$, ** $P < 0.01$ and *** $P < 0.001$.

Results

Satellite microglia can be identified in acute brain slices with bright field microscopy and are not dye-coupled with other cells

In bright field microscopy we could identify EGFP-expressing microglial cell somata with and without close proximity to a neuronal soma throughout the brain. In the present study we focused on cortex (layers 2-5) and hippocampus (CA1, stratum pyramidale and stratum radiatum). To verify the bright field-based identification of satellite and non-satellite microglia, we filled microglia with biocytin via the patch pipette and subsequently prepared the slices for 3D confocal imaging (see Methods). We regularly found biocytin-filled satellite microglia in close juxtaposition to a NeuN-positive neuron (Fig. 1 A, C). In these cell pairs, we could identify the contact area of the attached membranes (see inserts in Fig. 1).

We could also identify biocytin-filled non-satellite microglia in the cortex and hippocampus (Fig. 1 B, D) and confocal imaging verified that their soma was not touching a neuronal soma. Confocal microscopy thus confirmed that bright field microscopy allows to reliably distinguish satellite from non-satellite microglia.

Satellite microglia did not demonstrate any dye-coupling to the attached neuron or to any other cell (n=14 cortex, n=9 hippocampus; Fig.1 A, C). In agreement with published results (Richter *et al.*, 2014) non-satellite microglia did also not show any dye transfer to other cells (n=6 cortex, n=6 hippocampus; Fig.1 B, D). Biocytin injected satellite microglial cells were also investigated under the electron microscope. Indeed all labelled cell somata were in close membrane contact to a neuronal soma (n=4, Fig. 2). Neurons were identified by typical morphological features such as prominent Nissl bodies, a nucleus appearing

homogeneous without lumps of chromatin and containing a fragmented nucleolus and no cytoplasmic fibrils which are the most prominent feature of astrocytes. Likewise, the light cytoplasm and the absence of clumped chromatin in the nucleus distinguish neurons from oligodendrocytes. We found no specialized structures within the neuron at the contact zone to the microglia.

Satellite and non-satellite microglia show similar membrane current patterns

To characterize the membrane properties of satellite versus non-satellite microglial cells, we applied a series of de- and hyperpolarizing voltage steps in whole-cell voltage-clamp recordings (Fig. 1, upper part). Current-voltage relationships were compared between satellite and non-satellite cells in cortex and hippocampus (CA1).

In general, both satellite and non-satellite microglial cells lacked strong voltage gated currents. Besides a small inward rectification, they showed a rather linear current-to-voltage curve and had a high input resistance of $3.6 \pm 0.3 \text{ G}\Omega$ ($n=34$ cortical cells). We did not observe any significant differences between satellite and non-satellite microglia in the cortex (Supp. Fig. 1 A, B, left side). In the hippocampus, satellite microglia were predominantly located in stratum pyramidale whereas non-satellite microglia were most abundant in stratum radiatum. There was a significant difference between current density and membrane capacitance of the two hippocampal microglial cell populations (Supp. Fig. 1 A, B): The cell capacitance of non-satellite microglial cells from stratum radiatum was slightly, but significantly higher ($29.3 \pm 1.0 \text{ pF}$; $n=37$) compared to satellite microglia from stratum pyramidale ($25.8 \pm 1.3 \text{ pF}$; $n=33$; $P<0.05$; Figure 3 B, right side).

Electrical activity of neurons and satellite microglia do not coincide

To test whether neuronal electrical activity affects the membrane potential of satellite microglia, we performed dual patch-clamp recordings of a neuron and its attached satellite microglia (Fig. 3 B, n=18). After establishing the whole cell recording configuration the microglial cell was held at -20 mV, the neuron at -70 mV and current profiles from both cell types were obtained to verify their identity (Fig. 3 A). Depolarization to potentials more positive than -40 mV triggered typical sodium inward currents in neurons. As described above, microglial cells were characterized by a high input resistance and had a small inward rectifying component at negative membrane potentials.

Spontaneous or evoked action potentials did not lead to any correlated changes in the microglial membrane potential (Fig. 3 C). Similarly, spontaneous postsynaptic potentials in the neuron did not coincide with electrical events in its satellite microglia. However, we observed fast spontaneous membrane depolarizations in some of the microglial cells which are described in detail below. These microglial depolarizations did not coincide with action potentials nor neuronal spontaneous synaptic activity (Fig. 3 D).

We next tested whether evoked local field potentials did alter satellite microglial membrane potential. We stimulated the Schaffer collaterals and recorded population spikes in CA1, stratum radiatum close to stratum pyramidale where we simultaneously recorded from satellite microglia in current clamp (Fig. 3 F). Since the resting membrane potential was at about -30 mV (Supp. Fig. 1A) constant current was injected to record at about -70 mV. Single stimulation pulses (n=10, Fig. 3 E, G) did not alter microglial membrane potential except for a small deflection which was not voltage dependent and thus due to the change

in the external field potential (Fig. 3 H, n=3). Again, we detected spontaneous microglial depolarizations but they were not evoked by single electrical stimulation (Fig. 3 G).

In conclusion, neurons and their attached satellite microglia both generate electrical activity, but these activities appear independent from each other.

Analysis of spontaneous potentials in satellite microglia

At -70 mV, spontaneous depolarizing events occurred in satellite microglial cells in the neocortex and hippocampal CA1. For further analysis we focused on satellite microglia residing in stratum pyramidale of the hippocampal CA1 which are quite abundant in this region due to the high density of neurons. Spontaneous events of 17 satellite microglia were analyzed, with a recording time of at least 5 minutes each and a total recording time of 172 min. Events were only counted if their amplitude was twice as big as the noise level (0.5-1.5 mV) of the recording.

The depolarizing events differed greatly with regard to their rise time, amplitude and decay time (Fig. 4 A). The time from baseline to peak was defined as rise time and the time from peak to baseline was defined as decay time. Histograms of normalized event frequencies of rise velocities (defined as amplitude divided by rise time) pooled from different microglial cells revealed two distinct populations: Fast rising events and slow rising events (Fig. 4 B, upper part). In contrast, decay velocities (defined as amplitude divided by decay time) showed a uniform distribution (Fig. 4 B, lower part).

In accordance with these findings, logarithmic plots of rise velocities could be fitted by two Gaussian distributions (Fig. 5 A, left side) with peaks at 0.03

mV/ms and 0.37 mV/ms. Decay times followed a single Gaussian distribution (not shown).

We then calculated thresholds for confidence intervals to separate the fast (Fig. 5 A, blue fitted curve) and slow rising events (Fig. 5 A, red fitted curve). Slow rising events had a 90 % confidence interval ranging from 0.009 to 0.08 mV/ms (median=0.03 \pm 0.0007 mV/ms) whereas the interval for the fast rising events ranged from 0.2 to 0.6 mV/ms (median=0.37 \pm 0.007 mV/ms). All events with a rise velocity faster than 0.2 mV/ms (T_f , lower threshold for fast rising events) were counted as fast rising events and all events slower than 0.08 mV/ms (T_s , upper threshold for slow rising events) were counted as slow rising events.

With these criteria for separation, we generated scatter plots relating event amplitude of fast and slow rising events versus rise time and versus decay time (Fig. 5 B). The median amplitude of fast rising events was significantly higher than the median amplitude of slow rising events (4.2 \pm 0.20 mV and 2.2 \pm 0.05 mV, respectively, $P < 0.0001$; Fig. 5 C, Table 1).

We analyzed the frequencies of fast and slow rising event populations on a single cell level. The ratio of fast rising event frequency (from the recordings of all cells) to slow rising event frequency was 0.58.

Whereas every satellite microglia had slow rising spontaneous activity, fast rising events appeared in only 10 out of 17 cells with a mean frequency of 4.7 \pm 4.4 events/min. However, event frequency differed greatly between cells and only 1 out of the 10 active cells had a frequency above 1 min⁻¹ (44.1 events/min). Therefore cells with high frequency of fast events are indeed outliers but are best suited to study these events.

In conclusion, two types of spontaneous depolarizing events can be distinguished in satellite microglia: Fast rising events with a fast rising phase

typically had a higher amplitude compared to slow rising events displaying a slow rising phase and a lower amplitude.

Pharmacological modulation of spontaneous potentials in satellite microglia

We further tested whether we could pharmacologically interfere with the frequency of spontaneous events. For these experiments, we used satellite microglia with fast and slow rising event frequencies of at least 0.5 min^{-1} each, yielding higher baseline values of event frequency than given for the whole population above. As mentioned above, fast rising events do not occur in all cells and rarely with a high frequency. Therefore a large number of cells was analyzed until recordings of an adequate number of cells with fast spontaneous potentials in reasonable frequencies (0.5 min^{-1}) were obtained.

Bath application of the sodium channel blocker tetrodotoxin (TTX, $1\text{-}2 \text{ }\mu\text{M}$) did not significantly alter the frequency or kinetics of spontaneous microglial events ($n=4$, Supp. Fig. 2 A). We then added the NMDA- and AMPA-receptor antagonists D-APV ($50 \text{ }\mu\text{M}$) and CNQX ($20 \text{ }\mu\text{M}$) in the presence of TTX. Again, microglial electrical activity was not altered significantly ($n=4$, Supp. Fig. 2 A).

Since purinergic signaling plays a pivotal role in microglial physiology we applied a cocktail of P2X and P2Y receptor antagonists (TNP-ATP ($2 \text{ }\mu\text{M}$), Reactive Blue ($100 \text{ }\mu\text{M}$) and PPADS ($100 \text{ }\mu\text{M}$)). However, these blockers did also not affect microglial event frequencies ($n=4$, Supp. Fig. 2 B).

We next applied GABA because it has been shown to indirectly affect membrane currents in postnatal, amoeboid microglia (Cheung et al., 2009) and functional GABA_B receptors are expressed in microglia of acute mouse brain

slices (Kuhn et al., 2004). Moreover, Nimmerjahn et al., 2005, reported that GABA receptor antagonists alter microglial process motility.

Bath application of GABA (1 mM) reduced the mean frequency of the fast rising events from $3.6 \pm 1 \text{ min}^{-1}$ to $1.3 \pm 0.7 \text{ min}^{-1}$ ($P < 0.01$, $n=8$) at 2 min after application. This effect was reversible since the mean event frequency recovered to $3.8 \pm 1.4 \text{ min}^{-1}$ ($n=8$, $P < 0.05$) after washout of GABA (Fig. 6 B, left and upper right). The modulating effect of GABA was restricted to fast rising events while the frequency of slow rising potentials was unaffected (Fig. 6 B, right). Kinetics of the spontaneous potentials was not significantly altered by GABA. GABA did not change the membrane potential as indicated by the constant holding current required to keep the cell at -70 mV.

Spontaneous depolarizing activities in non-satellite microglia

After analyzing the spontaneous microglial potentials in satellite microglia we investigated whether they also occur in non-satellite microglia. Therefore, we recorded from non-satellite microglial cells in stratum radiatum of the CA1 region of the hippocampus ($n=18$, 182 min total recording time, Suppl. Table 1). Using the same recording protocol and statistical analysis as described above, we detected fast and slow rising events that could be separated with thresholds of 0.1 mV/ms (T_s) and 0.16 mV/ms (T_f). Fast rising events were found in 10 out of 18 non-satellite microglia with a mean event frequency of $3.4 \pm 2.1 \text{ min}^{-1}$.

When comparing non-satellite with satellite microglia we found that the rise velocities of fast rising events were significant lower in non-satellite microglial cells as compared to satellite microglia (0.25 ± 0.007 and $0.37 \pm 0.007 \text{ mV/ms}$, respectively, $P < 0.0001$; Table 1). Moreover, we found that the median amplitude

of fast rising events in non-satellite microglia was significantly lower than in satellite microglia (2.5 ± 0.1 mV and 4.2 ± 0.2 mV, respectively, $P < 0.0001$).

Voltage dependence of spontaneous events in satellite and non-satellite microglia

Voltage-dependence of spontaneous events was analyzed in recordings pooled together from satellite and non-satellite microglial cells. As described above we calculated confidence intervals and rise velocity thresholds for the slow and fast rising events for the pooled data, of 0.09 mV/ms and 0.18 mV/ms, respectively (see Table 1). Fast rising potentials were detected only at negative membrane potentials below -40 mV and we therefore restricted the analysis to membrane potentials ranging from -60 mV to -100 mV (Fig. 7). Slow rising potentials were also seen at more positive values. We compared the amplitude of fast and slow rising events at different membrane potentials ranging from -60 mV to -100 mV (Fig. 7). Below -60 mV fast rising event amplitudes were significantly higher than amplitudes of slow rising events and displayed a bell shaped voltage dependency with a maximum at -80 mV (3.5 ± 0.13 mV, Fig. 7). In contrast, slow rising event amplitudes decreased with more negative holding potentials with a minimum at -90 mV (1.4 ± 0.24 mV).

In addition we tested whether spontaneous microglial potentials are chloride sensitive. Therefore we performed ion substitution experiments with a low chloride intracellular solution which resulted in a chloride reversal potential of -70 mV. Cortical and hippocampal cells were patched and the membrane potential was set to -70 mV by constant current injection. Changes in microglial membrane potentials were measured in current clamp mode as described above. We found slow rising potentials in all recordings and fast rising potentials

in only 4 of 9 cells with a low frequency of $0.39 \pm 0.2 \text{ min}^{-1}$ (minimum recording time of 5 min). Since fast and slow events were recorded at the reversal potential of chloride we conclude that they are not exclusively mediated by chloride membrane currents.

Spontaneous microglial potentials are not dependent on the sex of the animals

We used the thresholds for fast and slow events for all microglia (see Table 1) and separated all previously described events dependent on the sex of the animals from which the data was obtained. In both sexes we could indeed identify the populations of fast and slow events leading to the conclusion that the different spontaneous potentials in microglia occur independent of the sex. Slow events occurred with a frequency of 7.37 ± 1.67 in females and $7.14 \pm 1.25 \text{ min}^{-1}$ in males (not significant, $P=0.92$, $n=10$ vs 24). Fast events were recorded in 5 out of 10 cells from female mice and 14 out of 24 cells from male mice. The recorded event frequencies of fast events were 2.9 ± 2.8 in females and $4.7 \pm 3.3 \text{ min}^{-1}$ in males (not significant, $P=0.77$, $n=5$ vs 14).

Discussion

There is increasing evidence that microglial cells are involved in synaptic plasticity in the normal brain (for review see (Paolicelli *et al.*, 2011; Kettenmann *et al.*, 2013; Schafer *et al.*, 2013)). It is now well established that microglial cells express functional neurotransmitter receptors and thus have the capacity to sense neuronal activity. Microglial cells express, for instance, receptors for GABA, glutamate, noradrenaline, ATP, serotonin or dopamine (Noda *et al.*,

2000; Boucsein *et al.*, 2003; Kuhn *et al.*, 2004; Farber *et al.*, 2005; Cheung *et al.*, 2009; Krabbe *et al.*, 2012; Beppu *et al.*, 2013).

Whereas the diversity of neurons in the brain is well studied little is known about the functional and morphological diversity of microglia within a given brain region or between different brain regions (Gertig & Hanisch, 2014; Doorn *et al.*, 2015). In the present study we have focused on a particular type of microglial cell, the satellite microglia. Satellite microglial cells are characterized by very close somatic contact to a neuron first described nearly a century ago by Pío del Río Hortega. Due to this attachment, satellite microglia somata had an aspherical shape as compared to non-satellite microglia. We found, however, no ultrastructural specializations at these microglial-neuronal contact sites.

This close apposition prompted us to analyze whether these satellite microglial cells might sense neuronal activity by simultaneously recording from such cell pairs. We found no electrical cross-talk between these two cell types. Neither neuronal evoked or spontaneous action potentials nor synaptic activity led to any correlated electrical activity in the adjacent microglia. Conversely we found no correlated neuronal responses to the spontaneous electrical activity which we describe here for the first time in microglial cells. Likewise evoked local field potentials triggered by single electrical stimulations only induced capacitive changes in the microglial membrane potential but no transmembrane currents.

Biocytin injection into satellite microglia remained confined to the injected cell indicating that also functional gap junctions are not present confirming previous studies in microglia not characterized as satellite microglia (Richter *et al.*, 2014; Wasseff & Scherer, 2014).

Recently a subset of satellite microglia cells was described in the cortex which is associated with the initial axonal segment termed AXIS microglia (Baalman *et*

al., 2015). This cell comprises about 8 % of total cortical microglia and this structural interaction is lost after microglial activation in pathology. The authors speculate that microglial cells might sense neuronal activity. Wu and Zhuo (2008), however, reported that stimulation of Schaffer collaterals in the CA1 region of the hippocampus does not lead to changes in membrane potential nor did they record any electrical activity in microglia. So far, we also could not obtain any evidence of electrical neuron-microglia crosstalk.

Even though we found no evidence of any electrical cross-talk between neurons and microglia, we recorded an intrinsic electrical activity in satellite and non-satellite microglia. These spontaneous depolarizations were recorded in current clamp and in particular the fast events were only observed at potentials negative to -40 mV. Wu and Zhuo (2008) however reported that neither single stimulation nor high frequency stimulation of Schaffer collateral evoked any changes in microglial membrane currents in stratum radiatum close to stratum pyramidale, nor did they observe any electrical spontaneous activity in microglia. We are confident that these events are intrinsically generated by the microglia and are not an experimental artifact. We observed these events at different electrophysiological setups both in Berlin and in Heidelberg using different types of patch-clamp amplifiers and recording devices and also recorded these events in a different mouse line (CX3CR^{-/-} and CX3CR^{+/-}, data not shown).

Microglial spontaneous events could be subdivided in two types depending on their rate of depolarization. In a logarithmic Gaussian distribution we found two distinct peaks in satellite microglia revealing median rise velocities of 0.03 and 0.37 mV/ms, respectively. We calculated thresholds to classify potentials

according to their rise velocity (Table 1). Fast rising events could only be recorded at membrane potentials negative to -40 mV, occurred rarely at -50 mV and frequently at -60 mV and more negative holding potentials. They have a characteristic time course with a fast rising phase and a slow decay phase. Moreover, they have a bell shaped nonlinear voltage dependency and were reduced in frequency by application of GABA. Since the GABA application did not alter the membrane potential of the microglial cell and we previously did not find evidence for GABA_A receptors expressed by microglial cells (Cheung *et al.*, 2009), we assume that this effect is rather due to inhibition of neuronal networks which leads to a secondary decrease in microglial event frequency.

On the other hand, slow rising events were also detected at potentials positive to -40 mV and displayed heterogeneous time courses. They exhibited a more linear voltage dependency and were insensitive to GABA and all other pharmacological substances tested. We therefore assume that these two events are based on different mechanisms.

We could exclude that the currents are mediated by chloride or potassium only, since we observed the events both at the potassium and chloride reversal potential. These currents are thus most likely mediated by a cationic conductance mediated by sodium or calcium or by a mixed cationic conductance.

Both types of events were insensitive to the application of TTX indicating that they are independent of action potentials. They were also insensitive to the NMDA and AMPA receptor antagonists APV and CNQX. The P2X and P2Y receptor antagonists TNP-ATP, Reactive Blue and PPADS did also not affect microglial spontaneous activity.

We focused our investigation on satellite microglia in stratum pyramidale and non-satellite microglia in stratum radiatum of hippocampal CA1. Both microglial cell types displayed spontaneous fast and slow rising events with significant differences in rise velocity and amplitude but not in frequency. Moreover, we measured different mean current densities and membrane capacitances in satellite and non-satellite microglia. It must be taken into consideration that microglia of different hippocampal layers were compared which might contribute to the mentioned electrophysiological differences between satellite and non-satellite microglia.

We conclude that spontaneous microglial activity can be studied likewise in satellite and non-satellite microglia. The underlying mechanism of spontaneous microglial potentials remains an issue which needs to be addressed in the future.

Acknowledgments

This work was supported by Deutsche Forschungsgemeinschaft (SFB TRR 43) and Neurocure and a MD fellowship of the Boehringer Ingelheim Fonds to EW. The authors wish to thank Vitali Matyash for excellent technical assistance with microscopic imaging and Claus Bruehl for his valuable comments and technical assistance. Moreover, we would like to thank Niklas Meyer for experimental assistance. The authors have no conflict of interest.

Abbreviations. ACSF, artificial cerebrospinal fluid; C, capacity; CA, cornu ammonis; CNQX, 6-cyano-7-nitroquinoxaline-2,3-dione; CX3CR, chemokine receptor 3; 3D, 3 dimensional; DAB, 3,3' diaminobenzidine tetrahydrochloride; D-APV, D-(-)-2-amino-5-phosphonopentanoic acid; EGFP, enhanced green fluorescent protein; I, current; Mp, membrane potential; log, logarithm; n.s., not significant; p, probability; P2 receptor, ATP receptor; PBS, phosphate-*buffered* saline; PPADS, pyridoxalphosphate-6-azophenyl-2',4'-disulfonic acid; RT, room temperature; S, stratum; SEM, standard error of the mean/median; TNP-ATP, 2',3'-O-(2,4,6-trinitrophenyl)adenosine-5'-triphosphate tetra(triethylammonium) salt; TTX, tetrodotoxin; U, voltage; Tf, lower threshold for fast rising events; Ts, upper threshold for slow rising events

References

- Baalman K, Marin MA, Ho TS, Godoy M, Cherian L, Robertson C & Rasband MN. (2015). Axon initial segment-associated microglia. *J Neurosci* **35**, 2283-2292.
- Beppu K, Kosai Y, Kido MA, Akimoto N, Mori Y, Kojima Y, Fujita K, Okuno Y, Yamakawa Y, Ifuku M, Shinagawa R, Nabekura J, Sprengel R & Noda M. (2013). Expression, subunit composition, and function of AMPA-type glutamate receptors are changed in activated microglia; possible contribution of GluA2 (GluR-B)-deficiency under pathological conditions. *Glia* **61**, 881-891.
- Boucsein C, Kettenmann H & Nolte C. (2000). Electrophysiological properties of microglial cells in normal and pathologic rat brain slices. *Eur J Neurosci* **12**, 2049-2058.
- Boucsein C, Zacharias R, Farber K, Pavlovic S, Hanisch UK & Kettenmann H. (2003). Purinergic receptors on microglial cells: functional expression in acute brain slices and modulation of microglial activation in vitro. *Eur J Neurosci* **17**, 2267-2276.
- Cheung G, Kann O, Kohsaka S, Faerber K & Kettenmann H. (2009). GABAergic activities enhance macrophage inflammatory protein-1alpha release from microglia (brain macrophages) in postnatal mouse brain. *J Physiol* **587**,

753-768.

- Del Río Hortega P. (1919). El tercer elemento de los centros nerviosos I La microglia en estado normal II Intervención de la microglia en los procesos patológicos III Naturaleza probable de la microglia. *Bol de la Soc esp de biol* **9**, 69-120.
- Doorn KJ, Breve JJ, Drukarch B, Boddeke HW, Huitinga I, Lucassen PJ & van Dam AM. (2015). Brain region-specific gene expression profiles in freshly isolated rat microglia. *Frontiers in cellular neuroscience* **9**, 84.
- Farber K, Pannasch U & Kettenmann H. (2005). Dopamine and noradrenaline control distinct functions in rodent microglial cells. *Molecular and cellular neurosciences* **29**, 128-138.
- Gertig U & Hanisch UK. (2014). Microglial diversity by responses and responders. *Frontiers in cellular neuroscience* **8**, 101.
- Kettenmann H, Hanisch UK, Noda M & Verkhratsky A. (2011). Physiology of microglia. *Physiol Rev* **91**, 461-553.
- Kettenmann H, Kirchhoff F & Verkhratsky A. (2013). Microglia: new roles for the synaptic stripper. *Neuron* **77**, 10-18.
- Krabbe G, Matyash V, Pannasch U, Mamer L, Boddeke HW & Kettenmann H. (2012). Activation of serotonin receptors promotes microglial injury-

induced motility but attenuates phagocytic activity. *Brain Behav Immun* **26**, 419-428.

Kuhn SA, van Landeghem FK, Zacharias R, Farber K, Rappert A, Pavlovic S, Hoffmann A, Nolte C & Kettenmann H. (2004). Microglia express GABA(B) receptors to modulate interleukin release. *Molecular and cellular neurosciences* **25**, 312-322.

Lawson LJ, Perry VH, Dri P & Gordon S. (1990). Heterogeneity in the distribution and morphology of microglia in the normal adult mouse brain. *Neuroscience* **39**, 151-170.

Newell EW & Schlichter LC. (2005). Integration of K⁺ and Cl⁻ currents regulate steady-state and dynamic membrane potentials in cultured rat microglia. *J Physiol* **567**, 869-890.

Nimmerjahn A, Kirchhoff F & Helmchen F. (2005). Resting microglial cells are highly dynamic surveillants of brain parenchyma in vivo. *Science* **308**, 1314-1318.

Noda M, Nakanishi H, Nabekura J & Akaike N. (2000). AMPA-kainate subtypes of glutamate receptor in rat cerebral microglia. *J Neurosci* **20**, 251-258.

Pannell M, Szulzewsky F, Matyash V, Wolf SA & Kettenmann H. (2014). The subpopulation of microglia sensitive to neurotransmitters/neurohormones is modulated by stimulation with LPS, interferon-gamma, and IL-4. *Glia*

62, 667-679.

Paolicelli RC, Bolasco G, Pagani F, Maggi L, Scianni M, Panzanelli P, Giustetto M, Ferreira TA, Guiducci E, Dumas L, Ragozzino D & Gross CT. (2011). Synaptic pruning by microglia is necessary for normal brain development. *Science* **333**, 1456-1458.

Richter N, Wendt S, Georgieva PB, Hambardzumyan D, Nolte C & Kettenmann H. (2014). Glioma-associated microglia and macrophages/monocytes display distinct electrophysiological properties and do not communicate via gap junctions. *Neurosci Lett* **583**, 130-135.

Sasmono RT, O'Ceandly D, Pollard JW, Tong W, Pavli P, Wainwright BJ, Ostrowski MC, Himes SR & Hume DA. (2003). A macrophage colony-stimulating factor receptor-green fluorescent protein transgene is expressed throughout the mononuclear phagocyte system of the mouse. *Blood* **101**, 1155-1163.

Schafer DP, Lehrman EK & Stevens B. (2013). The "quad-partite" synapse: microglia-synapse interactions in the developing and mature CNS. *Glia* **61**, 24-36.

Tremblay ME, Lowery RL & Majewska AK. (2010). Microglial interactions with synapses are modulated by visual experience. *PLoS Biol* **8**, e1000527.

Wake H, Moorhouse AJ, Jinno S, Kohsaka S & Nabekura J. (2009). Resting

microglia directly monitor the functional state of synapses in vivo and determine the fate of ischemic terminals. *J Neurosci* **29**, 3974-3980.

Wasseff SK & Scherer SS. (2014). Activated microglia do not form functional gap junctions in vivo. *Journal of neuroimmunology* **269**, 90-93.

Wu LJ & Zhuo M. (2008). Resting microglial motility is independent of synaptic plasticity in mammalian brain. *J Neurophysiol* **99**, 2026-2032.

Figure Legends

Fig. 1 Morphology and membrane currents of satellite and non-satellite microglia in acute brain slices

First row: Sample current profiles from satellite (A, C) and non-satellite (B, D) microglia in the cortex (A, B) and hippocampus (C, D). Currents were recorded in response to de- and hyperpolarizing voltage steps from -160 to +20 mV for 50 ms at a holding potential of -70 mV.

Second and third row: Confocal images of biocytin-injected microglia (red; microglia-biocytin/Cy3) without (second row) and with (third row) a neuronal marker (green; Alexa Fluo-488). Yellow (high magnification insert, black arrow) visualizes "digital fluo488/Cy3 fluorescence colocalization channel", and labels contact area between microglial and neuronal soma. Satellite microglial cells (A, C) are juxtaposed to a neuron while non-satellite microglia (B, D) are located within a visible distance to neighboring neurons. None of the biocytin-injected cells displayed dye-coupling with any other cell. Inserts in A and C show enlarged images of microglia (mg) and its satellite neuron (n). The scale bars denote 20 μm .

Fourth row: Rendered confocal 3D images show NeuN-positive neurons (green, A, C), non-satellite NeuN-positive neurons (grey, A-D) and biocytin-injected microglia (red). Scale bars denote 5 μm .

Fig. 2 EM image of a biocytin labeled satellite microglial cell and its associated neuron

A. Overview with a biocytin-filled cortical satellite microglial cell (dark grey).

B. Higher magnification of the biocytin-filled cell (dark grey). The cell membranes of the microglia and the neuron make physical contact. Note that there are no apparent structures at this contact site. Scale bars denote 5 μm . Nu, nucleus; p, perikaryon; NB, Nissl body.

Fig. 3 Electrical activity of neurons and satellite microglia do not coincide

A: Sample current profiles of a neuron (red traces) and its satellite microglia (black traces). The holding potential was -70 mV for neurons and -20 mV for microglia and the cells were depolarized to a series of de- and hyperpolarizing potentials as described in the legend to Fig. 1. Traces of neurons are depicted in red, traces from microglial cells in black. B: Bright field view (upper image) of the patched neuron (N) and its satellite microglia (M) and epifluorescence image of SR101 (lower image) after dialysis of the cells via the patch pipettes. Scale bar denotes 10 μm . C, D: Constant current was injected into the microglial cell to hyperpolarize the membrane to about -70 mV. Microglial membrane potential (black traces) did not change upon spontaneous (C, upper part) or induced (C, lower part) action potentials (red traces). D: Neuronal synaptic spontaneous activity (red traces) does not affect microglial membrane potential. Note that also spontaneous activity in microglial was observed which did not show any correlated changes in neuronal membrane potential. E: Electrical stimulation of the Schaffer collaterals evoked a population spike (red trace) and a small deflection (indicated by an asterisk) in the membrane potential of the satellite microglia (black trace). F: Bright field view of the stimulation pipette (Stim), the patch pipette (Patch) and the extracellular field electrode (Rec). Both the stimulation and the field electrode are located in the stratum radiatum and the patch pipette in the stratum pyramidale of the

hippocampal CA1. G: A spontaneous microglial depolarization not correlated with a single electrical stimulation. H: A microglia was clamped at membrane potentials ranging from -80 to +40 mV in 20 mV increments in voltage clamp mode during electrical stimulation of the Schaffer collaterals. Note that the amplitude of the current response correlated with the electrical stimulation was not voltage dependent.

Fig. 4 Spontaneous depolarizations in satellite microglia

A: Four examples of spontaneous depolarizations are shown with different rise velocities (in mV/ms; 1: 0.016; 2: 0.041, 3: 0.364, 4: 0.515). B: Histograms of the rise velocities (upper part) and decay velocities (lower part). Note that two distinct populations (fast and slow rising potentials) of events can be identified for the rise velocity.

Fig. 5 Analysis of spontaneous depolarizations in satellite microglia

A: Histogram of logarithmic rise velocities (left histogram, from the data shown in Fig. 4) with fitted Gaussian curves. From these fits, thresholds for 90 % confidence intervals were calculated for the slow rising events (red) and the fast rising events (blue). We took the exponent of the thresholds (T_f , lower threshold for fast rising events; T_s , upper threshold for slow rising events) to separate the two populations of the rise velocities (right histogram). B: Scatter blots depicting rise and decay times vs amplitudes. Note that the events can be separated in two groups by their rise time but not decay time (blue dots represent fast rising events, red dots represent slow rising events). C: Histograms depicting amplitudes of fast rising (left) and slow rising (right) velocities show that fast rising events have a higher median amplitude than slow rising events.

Fig. 6 The frequency of spontaneous microglial potentials is modulated by GABA

A: Example traces of a satellite microglial cell in current clamp mode (-70 mV) are shown before (left), during GABA (1 mM) application (middle) and after wash-out (right). Fast rising potentials are marked (■). B: Left diagram: Average frequencies of fast rising events of the eight tested satellite microglia are shown before, during GABA application and after wash-out. Right diagram: Average event frequencies for fast (blue, upper diagram) and slow (red, lower diagram) spontaneous potentials are shown upon GABA application. Only the fast rising event frequency was significantly and reversibly reduced from $3.6 \pm 1 \text{ min}^{-1}$ to $1.3 \pm 0.7 \text{ min}^{-1}$ (n=8, P<0.01,).

Fig. 7 Voltage dependency of spontaneous microglial potentials

Median amplitudes of slow (red) and fast (blue) events are shown at different membrane potentials ranging from -60 to -100 mV. At holding potentials below -60 mV the median amplitudes of the fast rising events are significantly higher compared to the slow rising events. Note the different voltage dependencies of the fast and slow rising events.

Supplementary information

Supplementary Fig. 1 Membrane properties of satellite and non-satellite microglia

A: Average current density (Im/Cm) versus voltage curve from satellite and non-satellite microglia of the cortex (left side, n=17 and n=17, respectively) and

hippocampus (right side, n=33 and n=37, respectively). Currents were recorded in response to de- and hyperpolarizing voltage steps from -160 to +20 mV for 50 ms at a holding potential of -70 mV.

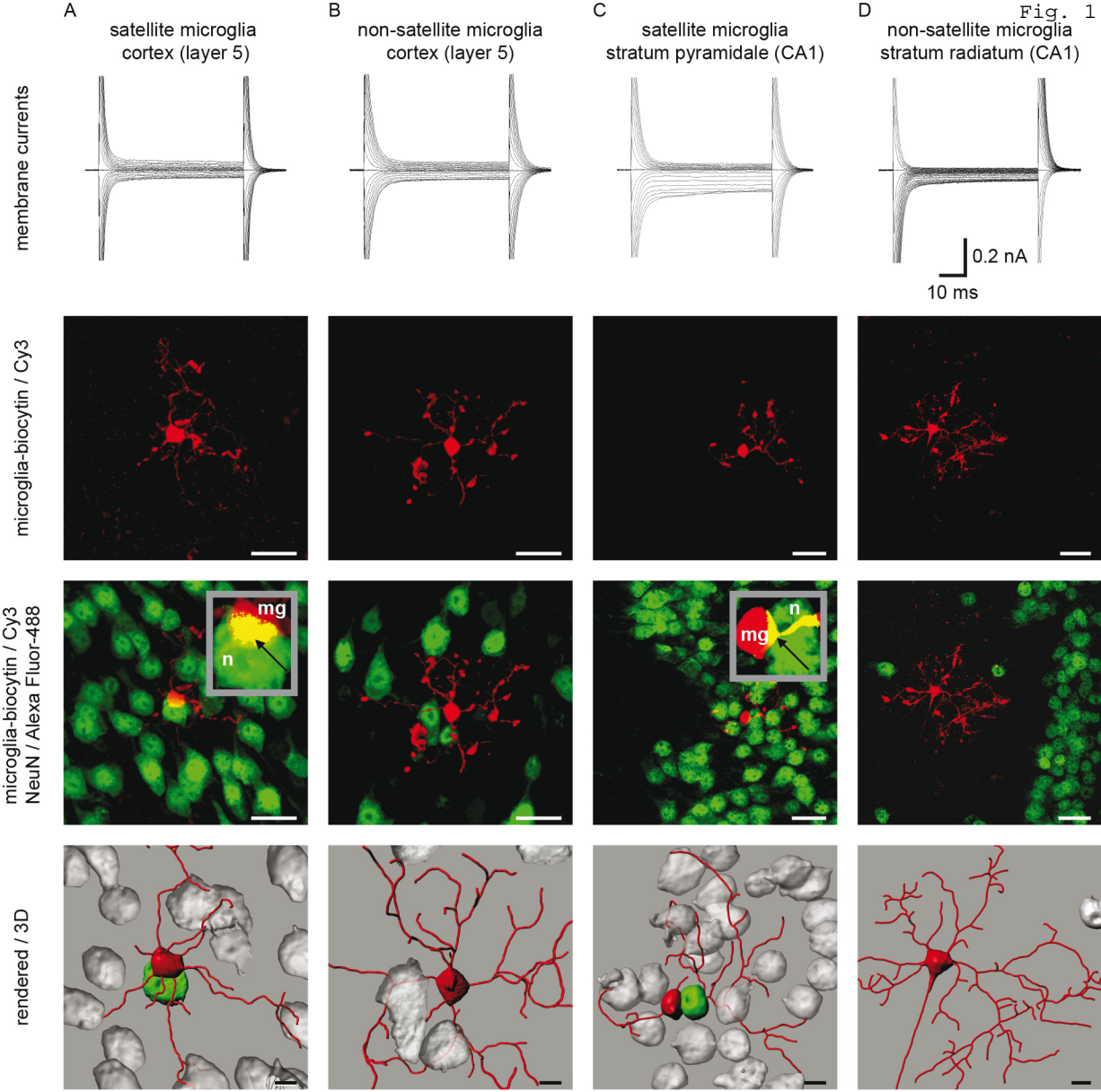
B: Average cell capacitance (C_m , upper part) and membrane potentials (M_p , lower part) of satellite and non-satellite microglia of the cortex (left side, n=17 and n=17, respectively) and hippocampus (right side, n=33 and n=37, respectively) are shown.

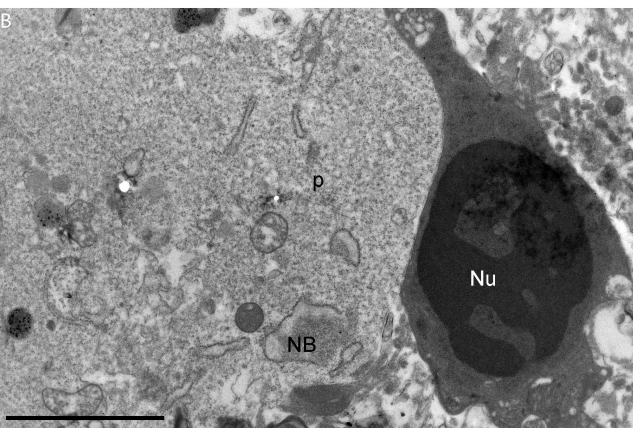
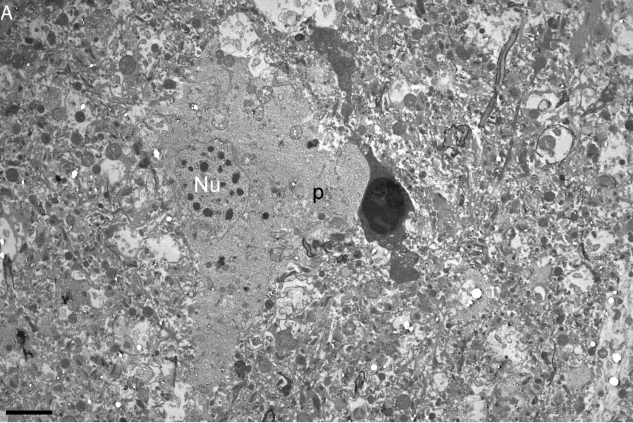
Satellite microglia from stratum pyramidale show higher current densities at -150 mV (-3 ± 0.3 to -2 ± 0.2 pA/pF; $P < 0.01$) and 50 mV (1.3 ± 0.12 to 0.9 ± 0.4 pF; $P < 0.01$) and decreased cell capacitance (25.8 ± 1.3 to 29.3 ± 1.0 pF; $P < 0.05$) compared to non-satellite microglia in stratum radiatum.

Supplementary Fig. 2 The effect of pharmacological substances on the frequency of spontaneous microglial potentials

A: Bath application of TTX did not significantly alter the frequency of fast (blue) and slow (red) rising microglial events. Subsequent application of APV and CNQX together with TTX did not significantly affect the event frequencies of the same cells (n=4).

B: In another set of cells a cocktail of TNP-ATP, Reactive Blue, PPADS did not alter microglial event frequencies (n=4).





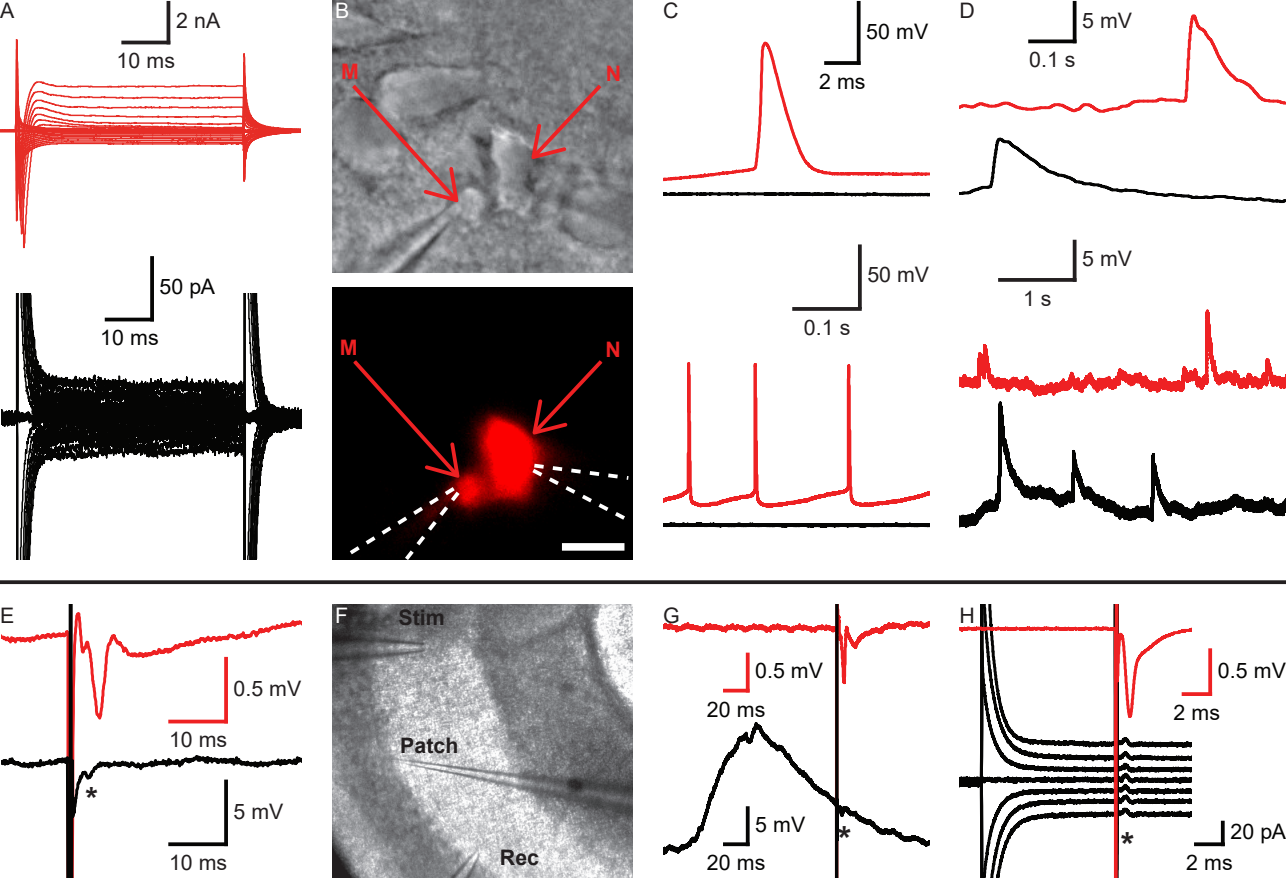
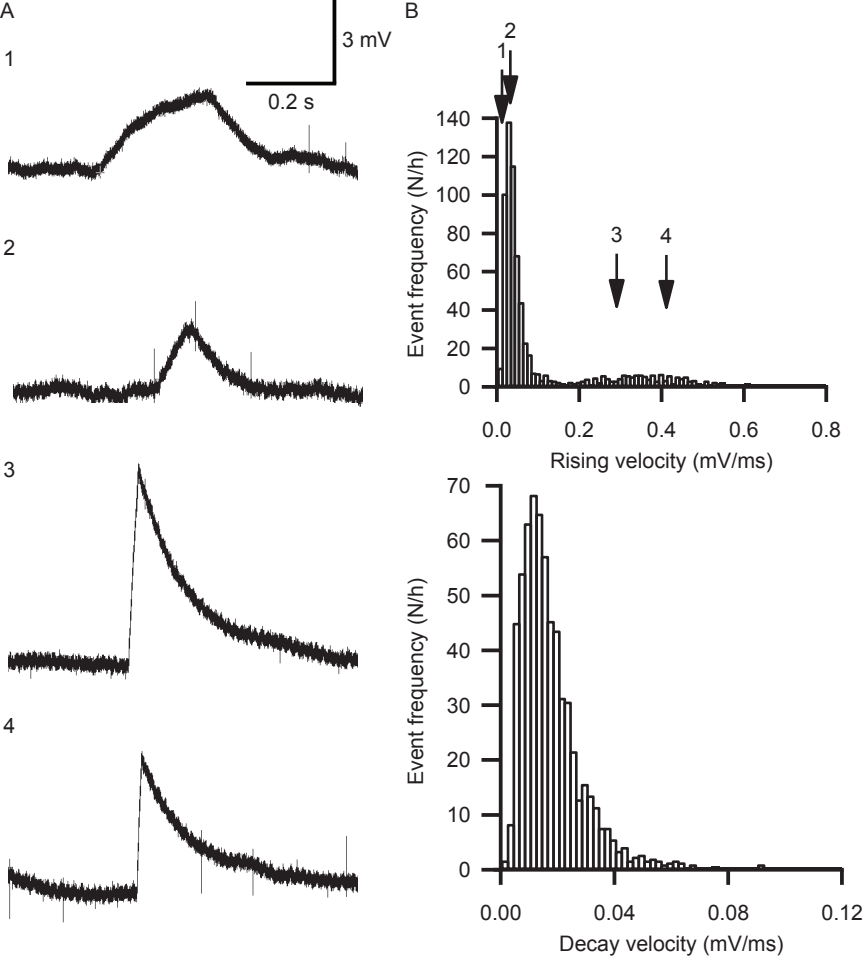
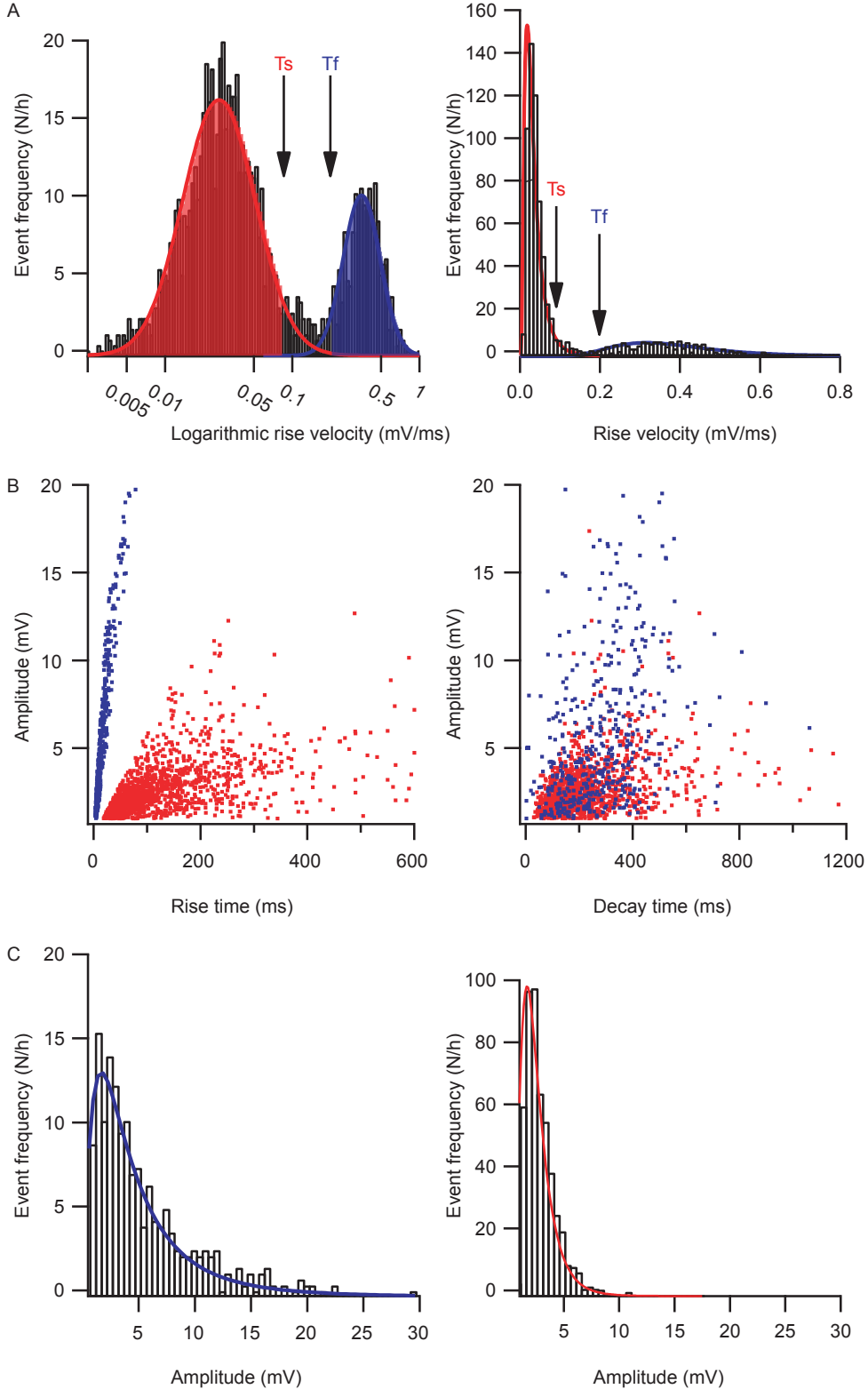
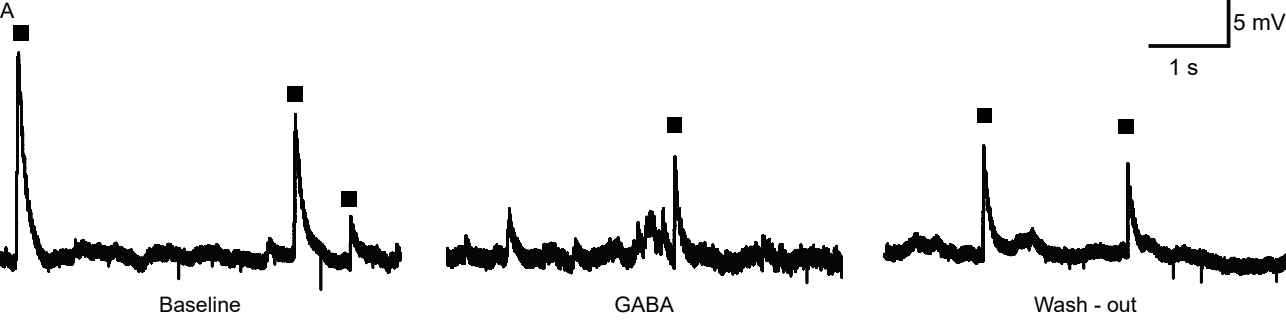


Fig. 3







B

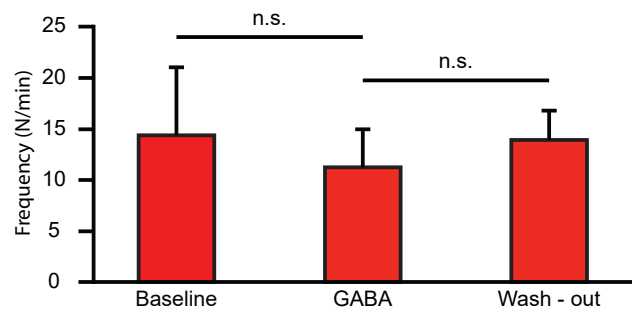
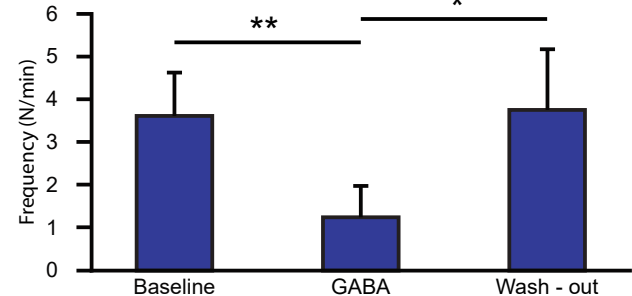
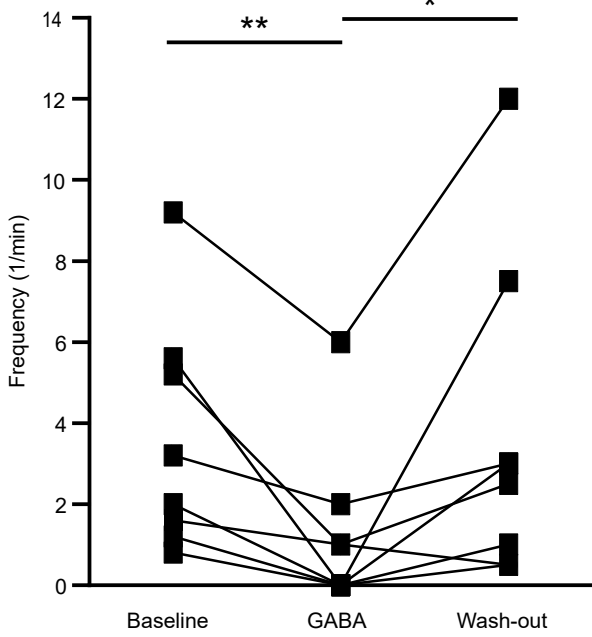


Fig. 6

Fig. 7

